

Geophysical Research Letters

RESEARCH LETTER

10.1029/2018GL081771

Key Points:

- We discover low-frequency tremor associated with Old Faithful from a dense seismic array deployed in 2016
- We employ seismic interferometry and back projection to locate the low-frequency tremor source in Old Faithful's deep plumbing structure
- We illuminate Old Faithful's fluid pathway down to ~80-m depth, tracking the phase transition horizon throughout the eruption cycle

Supporting Information:

- Supporting Information S1
- Movie S1
- Movie S2
- Movie S3
- Movie S4

Correspondence to:

S.-M. Wu,
sinmei.wu@utah.edu

Citation:

Wu, S.-M., Lin, F.-C., Farrell, J., & Allam, A. (2019). Imaging the deep subsurface plumbing of Old Faithful geyser from low-frequency hydrothermal tremor migration. *Geophysical Research Letters*, 46. <https://doi.org/10.1029/2018GL081771>

Received 20 DEC 2018

Accepted 14 JUN 2019

Accepted article online 24 JUN 2019

Imaging the Deep Subsurface Plumbing of Old Faithful Geyser From Low-Frequency Hydrothermal Tremor Migration

Sin-Mei Wu¹ , Fan-Chi Lin¹ , Jamie Farrell¹ , and Amir Allam¹ 

¹Department of Geology and Geophysics, University of Utah Salt Lake City, UT, USA

Abstract Old Faithful Geyser in Yellowstone is one of the most well-known hydrothermal features in the world. Despite abundant geophysical studies, the structure of Old Faithful's plumbing system beneath ~20-m depth remained largely elusive. By deploying a temporary dense three-component geophone array, we observe 1–5 Hz low-frequency hydrothermal tremor originating from Old Faithful's deeper conduit. By applying seismic interferometry and polarization analyses, we track seismic tremor source migration throughout the eruption/recharge cycle. The tremor source drops rapidly to ~80-m depth right after the eruption and gradually ascends vertically back to ~20-m depth, coinciding with the previously inferred bubble trap location. Likely excited by the liquid/steam phase transition, the observed tremor source migration can provide new constraints on the recharge process and deeper conduit geometry. Combined with the shallow conduit structure from previous studies, these results provide constraints on the major fluid pathway down to 80-m depth.

Plain Language Summary The fluid pathways beneath a geyser exert direct control over its eruption behavior. The conduit geometry not only serves as a pathway for fluid and mass transportation but also creates a distinct pressure gradient from the deep reservoir to the surface vent. Understanding the complete conduit geometry and the physical state of the hydrothermal fluid within it directly constrains the recharge and eruption dynamics. The deep plumbing system, however, is extremely challenging to probe based on in situ geophysical methods. Despite its fame and well-known nearly regular eruption intervals, the plumbing structure of Old Faithful Geyser in Yellowstone below 20-m depth remains largely elusive. In this study, we use data from a dense array of three-component seismometers to track the time-lapsed locations of low-frequency hydrothermal tremor, which is likely the result of pressure perturbations from the steam/liquid phase transition within the fluid column, throughout Old Faithful's eruption cycles. The results illuminate the fluid pathways of Old Faithful between ~20- and 80-m depth and provide critical constraints on the eruption dynamics of Old Faithful.

1. Introduction

The Upper Geyser Basin (UGB) in Yellowstone National Park provides optimal conditions for geyser formation: a persistent heat source, abundant water supply, and a ~65-m thick permeable glacial deposit overlying rhyolite flows (Abedini et al., 2015; Christiansen, 2001; Fenner, 1936; Muffler et al., 1982). The deep hydrothermal fluid derives its heat from the upper-crustal magma reservoir, with fluid migrating through permeable geologic strata, and interacting with the shallower and cooler ground water (Bouligand et al., 2019; Farrell et al., 2014; Hurwitz & Lowenstern, 2014; Wu et al., 2017). A narrow fluid pathway with a continuous heat influx from below can lead to an unstable two-phase-flow system where minor pressure perturbations (e.g., due to preplay) can trigger geyser eruptions (Hurwitz & Manga, 2017; Hutchinson et al., 1997; Kieffer, 1984). A detailed understanding of the plumbing system is required to build an accurate dynamic geyser model (Adelstein et al., 2014; Namiki et al., 2016; O'Hara & Esawi, 2013; Rudolph et al., 2018; Rudolph & Sohn, 2017).

Old Faithful Geyser, within the UGB, is one of the most studied geysers in the world (Hurwitz & Manga, 2017; Kieffer, 2017) not only due to its fame from the near-regularity of its ~90- to 100-min eruption interval but also because it is relatively distant from nearby hydrothermal features (Kieffer, 1984; Wu et al., 2017). An earlier study used in situ cameras along with temperature and pressure probes to study the shape, water level, and temperature variations within the shallow fissure-like conduit down to 21-m depth

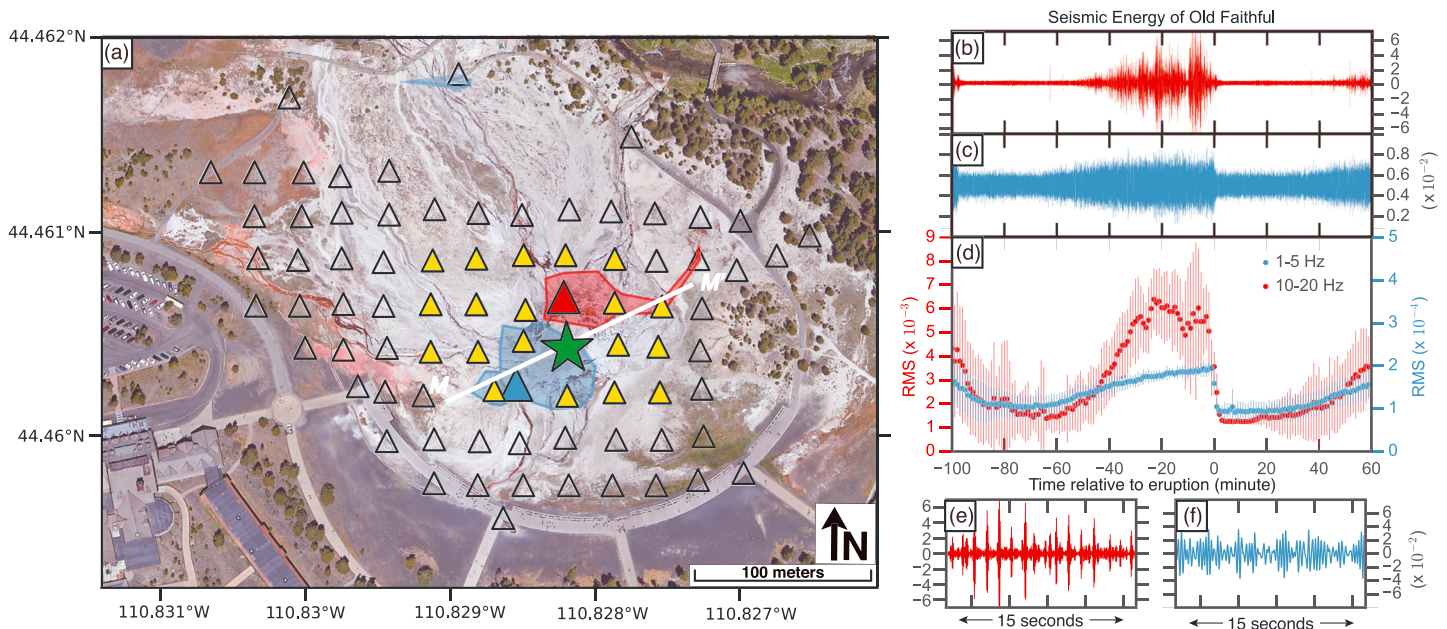


Figure 1. (a) The 80 station seismic array (triangles) within 200 m from Old Faithful's vent (star). Color-filled triangles denote the stations used for the back projection analysis. Stations with the strongest high-frequency (10–20 Hz, red triangle) and low-frequency (1–5 Hz, blue triangle) seismic root-mean-square (RMS) energy associated with the geyser activity are identified. The red and blue patches also illustrate the overall areas where high RMS of high-frequency and low-frequency signals are observed. The white line (M–M') shows the cross section in Figure 3a. (b) Example of 10–20 Hz vertical ground velocity during one eruption cycle recorded by the red triangle station shown in Figure 1a. The time scale is relative to Old Faithful's eruption time. (c) Same as Figure 1b but for 1–5 Hz and the blue triangle station shown in Figure 1a. (d) The average (dots) and standard deviation (error bars) of the RMS for the two frequency bands and the two example stations over 25 eruption cycles. (e and f) Same as Figures 1b and 1c but for a 15-s time window about 7 min before the eruption.

(Hutchinson et al., 1997). The eruption dynamics were proposed to be controlled by a narrow 11-cm conduit (chokepoint) 6.8 m below the geyser surface vent (Kieffer, 1989).

Though in situ probes can measure the exact physical state of a geyser's architecture, they are limited with respect to the lateral and deeper extent of the system. To better understand subsurface structure and eruption dynamics, a dense ~60-m aperture seismic array was deployed in 1992 around Old Faithful (Kedar et al., 1996) and Vandemeulebrouck et al. (2013) used a beamforming technique (Cros et al., 2011) to locate the high-frequency (>10 Hz) hydrothermal tremor signals associated with bubble collapse events. The tremor sources were found dominantly within the shallow conduit directly beneath the Old Faithful vent but a secondary source location ~20 m southwest of the surface vent was also observed. Based on the oscillatory behavior of the seismic frequency, a large cavity or bubble trap structure was inferred with a diameter of ~20 m at ~15-m depth.

More recently, a larger aperture (~1 km) seismic array was deployed across the UGB in 2015 and Wu et al. (2017) revealed a region with a highly fractured and porous medium ~150 m southwest of the Old Faithful vent down to ~60-m depth. The medium is inferred as a hydrothermal reservoir and is predominantly located within the glacial deposit and close to the stratigraphic boundaries of the Biscuit Basin flow to the East and an older rhyolitic lava flow below ~65-m depth (Abedini et al., 2015; Christiansen, 2001; Fenner, 1936; Muffler et al., 1982). The depth and the geologic controls on the formation of the medium have outlined the geological environment of Old Faithful and imply the possible depth extent (>20-m depth) of Old Faithful's plumbing system. However, Wu et al. (2017) only focused on larger-scale structure and did not resolve the detailed connection between the shallow and deeper Old Faithful plumbing system, which is the focus of the present study.

2. Low-Frequency Seismic Energy

In November 2016 we deployed a dense three-component 80-geophone array with ~20-m spacing and a ~300-m aperture across Old Faithful (Figure 1a and Text S1 in the supporting information). The array

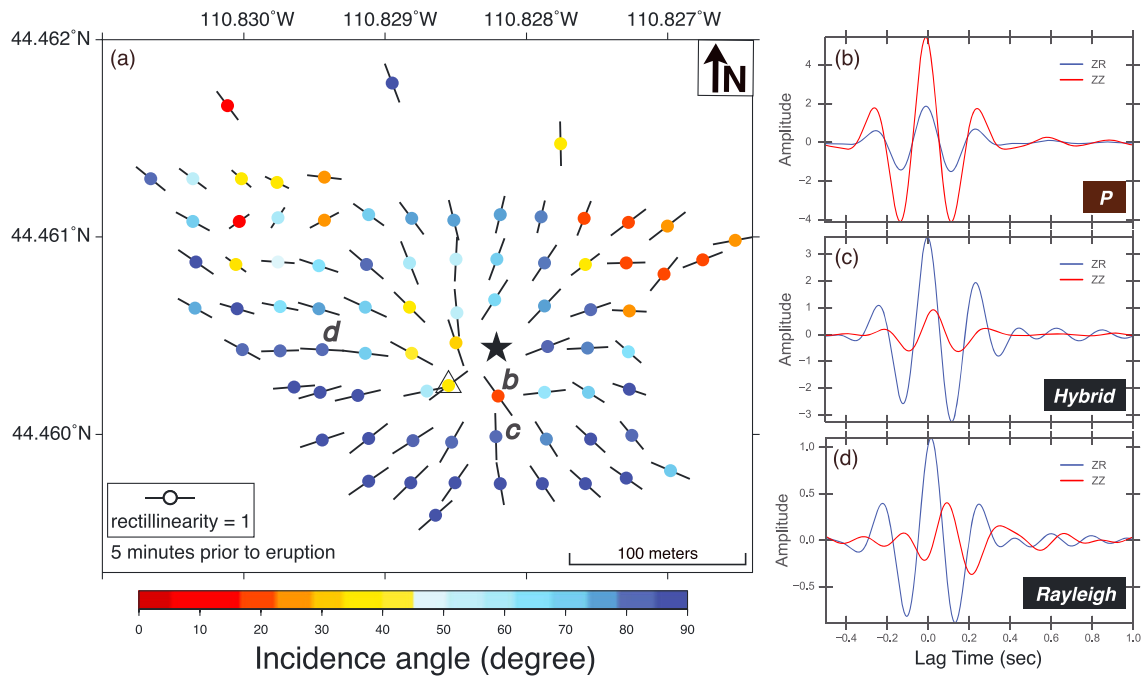


Figure 2. (a) The projection of 3-D direction to horizontal azimuth (bar) and incidence angle (color-coded circles, degrees relative to the vertical axis; blue and red represent nearly horizontal and vertical incidences, respectively). The black star denotes Old Faithful's location; the open triangle shows the location of the blue triangle shown in Figure 1a. The length of the bar represents the rectilinearity (i.e., the degree of being a straight line) defined in the polarization method (ranging from 0 to 1, the bottom-left panel indicates the rectilinearity equals to 1). (b–d) Examples of vertical-vertical (ZZ) and vertical-radial (ZR) cross-correlations at three different stations shown in Figure 2a. The radial direction is defined by the azimuth direction shown in Figure 2a.

recorded continuous data for 48 hours, which included over 25 eruptions. In addition to the >10-Hz high-frequency bubble collapse signals observed previously (Kedar et al., 1996, 1998; Kieffer, 1984; Vandemeulebrouck et al., 2013), we also observe low-frequency (1–5 Hz) hydrothermal tremor with distinct temporal and spatial variations (Figure 1). While the high-frequency energy has the strongest amplitude north of the surface vent, the low-frequency tremor is strongest to the southwest (Figure 1a). Unlike the high-frequency bubble collapse events that vary in seismic amplitude and precede eruptions (Kieffer, 1989; Rinehart, 1965), the low-frequency tremor amplitude consistently increases before each eruption but drops rapidly at the onset of an eruption (Figures 1b–1d). Finally, different from the high-frequency energy, the low-frequency energy contains no single distinctly identifiable events (Figures 1e–1f).

3. Tremor Source Migration

To understand the origin of the 1–5 Hz lower-frequency tremor, we use a seismic interferometry method (Bowden et al., 2015; Lin et al., 2014; Wu et al., 2017) to target the Old Faithful tremor signal and apply polarization analysis to evaluate the directionality and the dominant seismic wave type (Text S1; Allam et al., 2014; Vandemeulebrouck et al., 2014). First, we employ a multicomponent cross-correlation method to shift and align coherent seismic signals relative to the vertical-component signals observed at the station with the strongest low-frequency tremor energy (blue triangle in Figure 1a) during each 1-min time window. To further enhance the signal, we stack all 1-min cross correlations from different eruptions, using the eruption time as the reference. The stacking applied here amplifies the seismic signal by assuming a similar recharge pattern for each Old Faithful eruption. While abnormally short eruptions (<70-min eruption interval) do occur about once per day, ~90% of the 25 eruptions used in this study are regular eruptions (~93-min eruption interval) and have a highly consistent 1–5 Hz tremor pattern (Figure 1d). For each station and time relative to the eruption, the back azimuth and the incidence angle of the tremor energy is determined from the stacked three-component 1-min windowed cross-correlations, yielding a clear isotropic radiation pattern with a source centered ~20 m southwest of Old Faithful's vent (Figure 2a). For receivers close (<60 m) to Old Faithful's vent, clear rectilinear *P* wave motions are observed (Figure 2b). The seismic wavefield

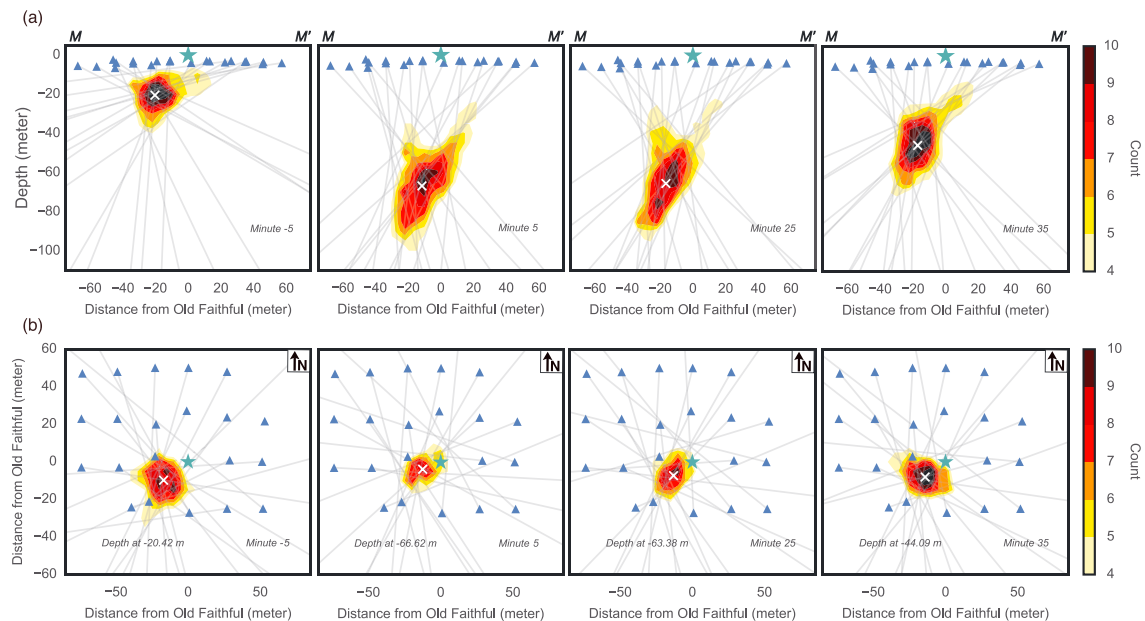


Figure 3. (a) Cross section of the back projected 1–5 Hz seismic energy following the M–M′ white line in Figure 1a. The star represents the location of Old Faithful. The triangles show the locations of stations. Each gray line illustrates the direction inferred at each station. The color-coded contours represent the density of the projected lines. The white crosses indicate the source locations determined by considering the mean location with hit counts above six. (b) Similar to Figure 3a but showing the map view of the projected line density around the source depth region.

transitions to elliptical Rayleigh wave motion (Figure 2d) at greater distances (~ 100 m), with hybrid motion (Figure 2c) observed at intermediate distances. We note that the cross-correlation waveforms observed at the northeastern and the northwestern corners of the array have overall low signal-to-noise ratios. In addition, those signals are highly inconsistent throughout the eruption cycle (Movie S1), which is likely affected by other hydrothermal features in the UGB (e.g., Wu et al., 2017). The strong localized *P* wave motion indicates that the tremor sources are located adjacent to Old Faithful’s cone within the shallow glacial and rhyolite deposits (<100 -m depth) and are likely related to vigorous volumetric perturbations.

Analysis of time-dependent changes in *P* wave incidence angles reveals systematic changes associated with the recharge cycle (Movie S1). To locate the low-frequency source as a function of time, we linearly back project the observed *P* waves along their corresponding incidence angle and back-azimuth (Figure 3 and Text S1). This back projection analysis assumes a homogeneous half space velocity model, which is a reasonable first-order approximation considering the relatively long-wavelength 1–5 Hz seismic energy. Prior to an eruption, the seismic source remains relatively stable at 20- to 25-m depth, but at the onset of eruption it descends rapidly to $\sim 80 \pm 10$ -m depth. After the eruption, the source migrates upward nonlinearly, with a clear rate change at ~ 58 -m depth, and reaches $\sim 22 \pm 6$ -m depth about 50 min after the eruption (Figures 3a and Figure 4a and Movie S2). Throughout this vertical migration, the horizontal tremor source locations remain ~ 20 m southwest of Old Faithful’s vent (Figure 3b and Movie S3), which coincides with the previously inferred bubble trap based on the high-frequency (>10 Hz) bubble collapse signals (Vandemeulebrouck et al., 2013).

4. Old Faithful Plumbing System

Assuming the 1–5 Hz seismic tremor signals originate from a steam/liquid phase transition within the water column, the time-lapsed tremor source migration throughout the eruption cycle illuminates, for the first time, the deeper Old Faithful fluid pathway (between 20- and 80-m depth; Figure 4c). Two distinct ascending rates are observed: the tremor source rises slowly (~ 0.6 m/min) for the first ~ 30 -min post-eruption (t_0 to t_1 in Figure 4), followed by a sharp change to a more rapid rate (~ 2 m/min; t_1 to t_2 in Figure 4). The ascending sources can be expressed with two distinct logarithmic relationships during Old Faithful’s recharge and with a clear slope change at 32-min post-eruption and at 58 ± 10 -m depth (Figure 4b). Assuming the tremor migration reflects a change in the phase transition horizon, we hypothesize that the observed rate change

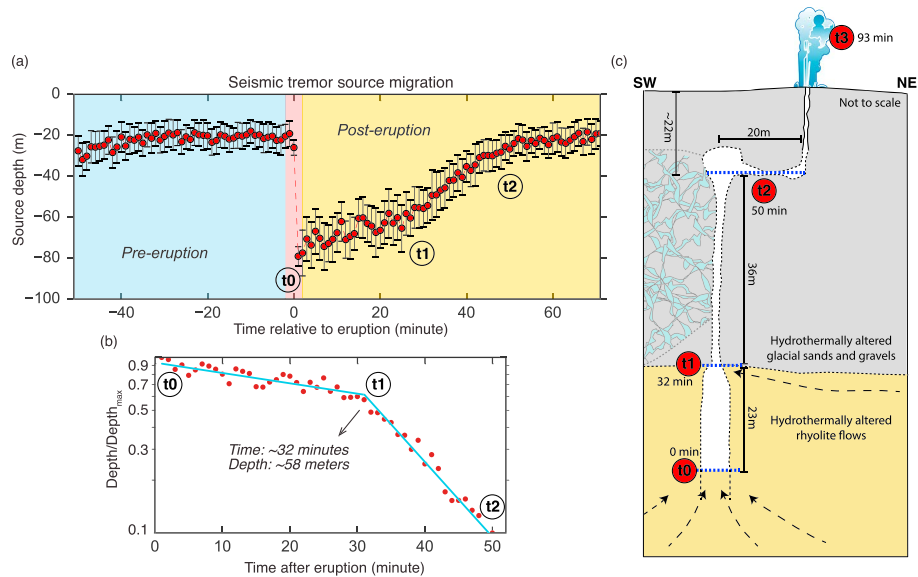


Figure 4. (a) Tremor source depth as a function of time with respect to the eruption cycle. The red circles show the depth of seismic sources, corresponding to the white crosses shown in Figure 3a. The error bars indicate the one standard deviation uncertainties in depth based on the area with hit counts above six. t_0 - t_2 : see the description in Figure 4c. (b) Similar to Figure 4a, but showing the normalized source depth ($\text{depth}/\text{depth}_{\text{max}}$) for the post-eruption regime in semilog space. The blue lines represent least squares fitting of the two linear trends. The labels exhibit the estimated time and depth for the rapid change of the source depth. (c) Hypothesized schematic model of Old Faithful Geyser's conduit and recharge evolution during an eruption cycle. The shallow conduit is constructed based on the results of previous studies (Hutchinson et al., 1997; Vandemeulebrouck et al., 2013). The times (t_0 : 0 min; t_1 : 32 min; t_2 : 50 min; t_3 : 93 min) are estimated based on a 93-min Old Faithful eruption cycle, starting immediately after the previous eruption, which also marks the dominant 1–5 Hz tremor source locations from this study. The 93-min eruption interval is the averaged interval among 25 eruptions used in this study. The narrowing of the deeper conduit around 58-m depth is hypothesized based on the change of the tremor migration rate around 32 min after the eruption. For reference, the larger-scale highly fractured and porous medium imaged by Wu et al. (2017) is also shown on the SW of Old Faithful, although the exact connection between the large-scale feature and the newly imaged lower conduit from this study remains unclear.

might be the result of a sudden narrowing of the conduit from deep to shallow, although additional heat influx and hydrostatic pressure variations could also contribute. As a narrower conduit has a lower volume, its temperature would increase faster with a constant heat influx. Interestingly, the sharp change of ascending rate at ~58-m depth is close to the stratigraphic boundary between the basal rhyolite and overlying glacial deposits. Previous geological drilling in a nearby site located this boundary at ~65-m depth (Fenner, 1936). Owing to the difference in permeability between the two geologic units, it is plausible that the same boundary marks a change in the plumbing geometry/dimension. It is also possible that additional hot hydrothermal fluids preferentially flow laterally along this boundary (Bouligand et al., 2019; Hurwitz & Lowenstern, 2014) and enter the Old Faithful conduit at this depth, providing an additional heat source.

The hydrothermal tremor source migration observed in this study combined with previous studies of the geyser system (Hutchinson et al., 1997; Vandemeulebrouck et al., 2013; Wu et al., 2017) provides a more comprehensive image of Old Faithful's plumbing system (Figure 4c). The lower conduit from ~20- to 80-m depth is approximately vertical and is offset ~20 m southwest of the geyser vent near the edge of a previously imaged larger-scale highly fractured and porous reservoir (Wu et al., 2017). While it is unclear if the larger-scale reservoir is involved directly with the eruption process, it likely contributes to the fast recharge of Old Faithful and insures the long-term stability of the eruption cycle. The top of the lower conduit coincides with the bubble trap structure (Vandemeulebrouck et al., 2013) that laterally connects to the ~21 m upper conduit revealed from in situ observations (Hutchinson et al., 1997). Although the lateral dimension of the lower conduit is not constrained in this study, we infer that the conduit geometry might be wider below ~58-m depth to explain the slower tremor migration immediately after the eruption.

5. Tremor Source Mechanism

Vandemeulebrouck et al. (2014) observed two dominant frequency bands (5–8 and 15–25 Hz) for the hydrothermal tremor at Lone Star Geyser in Yellowstone and discussed three possible mechanisms for the tremor-generating steam/liquid phase transition: bubble nucleation, bubble collapse at an interface, and bubble collapse in a subcooled liquid. The isotropic source pattern from seismic polarization analysis (Figure 2a) supports that the 1–5 Hz low-frequency tremor observed in this study is the result of volumetric source perturbations associated with a steam/liquid phase transition. Bubble collapse at the liquid/air interface seems to be an unlikely mechanism as that would suggest a sudden drop of the liquid water level to ~80-m depth right after the eruption. This is inconsistent with previous studies, which indicates the water was at ~16-m depth after an eruption (Hutchinson et al., 1997) with high-frequency tremor continuously being excited within the bubble trap at ~20-m depth immediately after an eruption (Vandemeulebrouck et al., 2013).

Previous studies at Old Faithful have associated the high-frequency tremor (>10 Hz) with bubble collapse when steam bubbles rise within the water column and are cooled by the colder shallower water (Kedar et al., 1998). A sudden pressure pulse in the water column due to steam bubble collapse can couple to the surrounding rock matrix and excite outgoing seismic waves (Kieffer, 1984; Rinehart, 1965). By using contemporary seismic and pressure probe measurements, Kedar et al. (1996) observed a direct correlation between high-frequency (>10 Hz) seismic signals and pressure pulses within the Old Faithful shallow conduit. Based on beamforming, Vandemeulebrouck et al. (2013) tracked the high-frequency tremor source migration between the offset bubble trap and shallow conduit.

If bubble collapse is also responsible for the 1–5 Hz tremor observed in this study, it is possible that the exact frequency content of the deep tremor signals is modified by path effects while the shallow medium preferentially attenuates and scatters higher frequency signals (Kedar et al., 1996). In this scenario, the depth at which steam bubbles are collapsing can drop rapidly to ~80-m depth after an eruption as the fluid within the geyser system dissipates a significant amount of its heat due to vigorous vaporization. The gradual migration of the source horizon could represent progressive heating during the recharge process where the rising bubbles contribute to the heating of the shallow system. Near the end of the recharge process, the tremor source location at ~20-m depth coincides with the previously inferred bubble trap which suggests that the fluid within likely reaches its saturation temperature and the system is primed for another eruption. In this scenario, it remains unclear how ~80-m deep low-frequency tremor coexists with previously observed shallow ~20-m deep high-frequency tremor (Vandemeulebrouck et al., 2013) in the immediate aftermath of an eruption; this will be the subject of future study.

An alternative source mechanism for the low-frequency tremor is bubble nucleation. At the onset of the eruption, the reduction of hydrostatic pressure within the whole conduit system can trigger a phase transition and vigorous steam bubble nucleation in the deeper conduit down to ~80-m depth. During the first ~50 min of the recharge process, the dominant nucleation area gradually rises from ~80- to ~20-m depth with an increase of the hydrostatic pressure and temperature within the plumbing system. We note that our polarization analysis allows us to locate the source of the dominant signals but cannot rule out the contemporary existence of other weaker sources. During the vertical migration of the low-frequency tremor, rising bubbles also collapse when they interact with shallow subcooled water in the shallow plumbing system, which excites contemporaneous high-frequency tremor in the bubble trap and shallow conduit (Figures 1b and 1d; Kedar et al., 1996; Kedar et al., 1998; Vandemeulebrouck et al., 2013). After ~50 min into the recharge process or ~40 min before the next eruption, the steam bubbles dominantly nucleate at ~20-m depth within the bubble trap when subcooled bubble collapse is observed in the shallow conduit beneath the geyser vent (Vandemeulebrouck et al., 2013). At this stage, the bubble trap likely contains a liquid/vapor two-phase mixture and small perturbations can trigger preplay observed on the surface (Vandemeulebrouck et al., 2013). At ~93 min after the previous eruption, the fluid within both the shallow and deeper conduits is likely close to the critical phase transition state, and a full eruption can occur.

6. Conclusion

In this study, we deployed a dense, three-component seismic geophone array in the vicinity of Old Faithful in November 2016. From the continuous seismographs, we discover previously undiscussed low-frequency

tremor (1–5 Hz) associated with Old Faithful's recharge dynamics. Incorporated with seismic interferometry and polarization techniques, our results illuminate a systematic tremor source migration from 80- to 20-m depth during Old Faithful's recharge process. The tremor is likely originated from the liquid/steam phase transition within Old Faithful's plumbing system, which indicates that the deep plumbing system (~20- to 80-m depth) is likely involved in the eruption dynamics of Old Faithful. From the source location of the tremor, we propose the deep conduit geometry is approximately vertical and offset ~20 m southwest of the geyser vent and the top of the conduit is collocated with a bubble trap feature inferred by Vandemeulebrouck et al. (2013). By tracking the ascending phase transition horizon during Old Faithful's recharge, we observe the migration follows two distinct logarithmic patterns with a clear abrupt rate change from slower to faster at 58 ± 10 -m depth, which is close to a stratigraphic boundary observed in a nearby borehole experiment (Fenner, 1936). We propose two scenarios to account for the abrupt rate change: (1) the deep conduit has an abrupt dimension change at 58 ± 10 -m depth. The upper portion (<58-m depth) is smaller in size, and the bottom portion (>58-m depth) is an enlargement structure and/or (2) additional lateral hydrothermal flow is preferentially directed to Old Faithful's deep plumbing system along that geologic boundary. Further numerical/physical modeling studies on the Old Faithful Geyser investigating the precise temporal and spatial relationship between the high- and low-frequency hydrothermal tremor can provide a better understanding of the complicated dynamic processes associated with its near-regular eruption cycles. A robust measure and comparison of tremor migration within other hydrothermal and volcanic systems will lead to greater understanding of the exact relationship between tremor migration and eruption mechanisms and enhance the potential to predict hydrothermal and analogous volcanic eruption systems (Chouet, 1996; Chouet & Matoza, 2013; Shapiro et al., 2017).

Acknowledgments

The authors thank Kip Solomon, Michael Manga, Shaul Hurwitz, and Jean Vandemeulebrouck for insights into hydrothermal systems. We thank Rob Sohn and an anonymous reviewer for constructive comments. We thank Bob Smith, Keith Koper, and Michael Ritzwoller for providing initial reviews of this paper. We also thank the Yellowstone National Park Center for Resources for providing collaborative support and field personnel. Data collection was performed under Yellowstone National Park permit YELL-2016-SCI-0114. We would like to thank Kevin Ward, Jonathan Delph, Andy Trow, Elizabeth Berg, Lisa Linville, Galen Kaip, Jose Cervantes, and Jonathan Lucero for help in the field deployment. In addition, we would like to thank Marianne Karplus at the University of Texas at El Paso for providing instrumentation for the deployment. This research is supported by NSF CyberSEES-1442665, EAR-1753362 and EAR-1760094 and the Brinson Foundation. The noise cross correlations used in this study can be downloaded from http://noise.earth.utah.edu/UGB_CCF_GRL_2019.tar.

References

- Abedini, A. A., Robinson, J. E., Muffler, L. P., White, D., Beeson, M. H., & Truesdell, A. (2015). Database for the geologic map of Upper Geyser Basin, Yellowstone National Park, Wyoming (No. 2327-638X): US Geological Survey.
- Adelstein, E., Tran, A., Saez, C. M., Shteinberg, A., & Manga, M. (2014). Geyser preplay and eruption in a laboratory model with a bubble trap. *Journal of Volcanology and Geothermal Research*, 285, 129–135. <https://doi.org/10.1016/j.jvolgeores.2014.08.005>
- Allam, A., Ben-Zion, Y., & Peng, Z. (2014). Seismic imaging of a bimaterial interface along the Hayward fault, CA, with fault zone head waves and direct P arrivals. *Pure and Applied Geophysics*, 171(11), 2993–3011. <https://doi.org/10.1007/s00024-014-0784-0>
- Bouligand, C., Hurwitz, S., Vandemeulebrouck, J., Byrdina, S., Kass, M. A., & Lewicki, J. L. (2019). Heat and mass transport in a vapor-dominated hydrothermal area in Yellowstone National Park, USA: Inferences from magnetic, electrical, electromagnetic, subsurface temperature, and diffuse CO₂ flux measurements. *Journal of Geophysical Research: Solid Earth*, 124(1), 291–309. <https://doi.org/10.1029/2018JB016202>
- Bowden, D., Tsai, V., & Lin, F. (2015). Site amplification, attenuation, and scattering from noise correlation amplitudes across a dense array in Long Beach, CA. *Geophysical Research Letters*, 42, 1360–1367. <https://doi.org/10.1002/2014GL062662>
- Chouet, B. A. (1996). Long-period volcano seismicity: Its source and use in eruption forecasting. *Nature*, 380(6572), 309–316. <https://doi.org/10.1038/380309a0>
- Chouet, B. A., & Matoza, R. S. (2013). A multi-decadal view of seismic methods for detecting precursors of magma movement and eruption. *Journal of Volcanology and Geothermal Research*, 252, 108–175. <https://doi.org/10.1016/j.jvolgeores.2012.11.013>
- Christiansen, R. L. (2001). The Quaternary and pliocene Yellowstone plateau volcanic field of Wyoming, Idaho, and Montana (No. 2330-7102).
- Cros, E., Roux, P., Vandemeulebrouck, J., & Kedar, S. (2011). Locating hydrothermal acoustic sources at Old Faithful Geyser using matched field processing. *Geophysical Journal International*, 187(1), 385–393. <https://doi.org/10.1111/j.1365-246X.2011.05147.x>
- Farrell, J., Smith, R. B., Husen, S., & Diehl, T. (2014). Tomography from 26 years of seismicity revealing that the spatial extent of the Yellowstone crustal magma reservoir extends well beyond the Yellowstone caldera. *Geophysical Research Letters*, 41, 3068–3073. <https://doi.org/10.1002/2014GL059588>
- Fenner, C. N. (1936). Bore-hole investigations in Yellowstone Park. *The Journal of Geology*, 44(2, Part 2), 225–315. <https://doi.org/10.1086/624425>
- Hurwitz, S., & Lowenstern, J. B. (2014). Dynamics of the Yellowstone hydrothermal system. *Reviews of Geophysics*, 52, 375–411. <https://doi.org/10.1002/2014RG000452>
- Hurwitz, S., & Manga, M. (2017). The fascinating and complex dynamics of geyser eruptions. *Annual Review of Earth and Planetary Sciences*, 45(1), 31–59. <https://doi.org/10.1146/annurev-earth-063016-015605>
- Hutchinson, R. A., Westphal, J. A., & Kieffer, S. W. (1997). In situ observations of Old Faithful geyser. *Geology*, 25(10), 875–878. [https://doi.org/10.1130/0091-7613\(1997\)025<0875:ISOOOF>2.3.CO;2](https://doi.org/10.1130/0091-7613(1997)025<0875:ISOOOF>2.3.CO;2)
- Kedar, S., Kanamori, H., & Sturtevant, B. (1998). Bubble collapse as the source of tremor at Old Faithful Geyser. *Journal of Geophysical Research*, 103(B10), 24,283–24,299. <https://doi.org/10.1029/98JB01824>
- Kedar, S., Sturtevant, B., & Kanamori, H. (1996). The origin of harmonic tremor at Old Faithful Geyser. *Nature*, 379(6567), 708–711. <https://doi.org/10.1038/379708a0>
- Kieffer, S. W. (1984). Seismicity at Old Faithful Geyser: an isolated source of geothermal noise and possible analogue of volcanic seismicity. *Journal of Volcanology and Geothermal Research*, 22(1-2), 59–95. [https://doi.org/10.1016/0377-0273\(84\)90035-0](https://doi.org/10.1016/0377-0273(84)90035-0)
- Kieffer, S. W. (1989). Geologic nozzles. *Reviews of Geophysics*, 27(1), 3–38. <https://doi.org/10.1029/RG027i001p00003>
- Kieffer, S. W. (2017). Researching the Earth—And a Few of its neighbors. *Annual Review of Earth and Planetary Sciences*, 45(1), 1–29. <https://doi.org/10.1146/annurev-earth-063016-020501>

- Lin, F.-C., Tsai, V. C., & Schmandt, B. (2014). 3-D crustal structure of the western United States: Application of Rayleigh-wave ellipticity extracted from noise cross-correlations. *Geophysical Journal International*, *198*(2), 656–670. <https://doi.org/10.1093/gji/ggu160>
- Muffler, L., White, D., Beeson, M., & Truesdell, A. (1982). *Geologic map of Upper Geyser Basin*. Wyoming: Yellowstone National Park.
- Namiki, A., Ueno, Y., Hurwitz, S., Manga, M., Munoz-Saez, C., & Murphy, F. J. G. (2016). An experimental study of the role of subsurface plumbing on geothermal discharge. *Geophysics, Geosystems*, *17*(9), 3691–3716. <https://doi.org/10.1002/2016GC006472>
- O'Hara, K. D., & Esawi, E. (2013). Model for the eruption of the Old Faithful geyser, Yellowstone National Park. *GSA Today*, *23*(6), 4–9. <https://doi.org/10.1130/GSATG166A.1>
- Rinehart, J. S. (1965). Earth tremors generated by Old Faithful geyser. *Science*, *150*(3695), 494–496. <https://doi.org/10.1126/science.150.3695.494>
- Rudolph, M. L., & Sohn, R. A. (2017). A model for internal oscillations in geysers, with application to Old Faithful (Yellowstone, USA). *Journal of Volcanology and Geothermal Research*, *343*, 17–24. <https://doi.org/10.1016/j.jvolgeores.2017.04.023>
- Rudolph, M. L., Sohn, R. A., & Lev, E. (2018). Fluid oscillations in a laboratory geyser with a bubble trap. *Journal of Volcanology and Geothermal Research*, *368*, 100–110. <https://doi.org/10.1016/j.jvolgeores.2018.11.003>
- Shapiro, N., Droznin, D., Droznina, S. Y., Senyukov, S., Gusev, A., & Gordeev, E. (2017). Deep and shallow long-period volcanic seismicity linked by fluid-pressure transfer. *Nature Geoscience*, *10*(6), 442–445. <https://doi.org/10.1038/ngeo2952>
- Vandemeulebrouck, J., Roux, P., & Cros, E. (2013). The plumbing of Old Faithful Geyser revealed by hydrothermal tremor. *Geophysical Research Letters*, *40*, 1989–1993. <https://doi.org/10.1002/grl.50422>
- Vandemeulebrouck, J., Sohn, R. A., Rudolph, M. L., Hurwitz, S., Manga, M., Johnston, M. J., et al. (2014). Eruptions at Lone Star geyser, Yellowstone National Park, USA: 2. Constraints on subsurface dynamics. *Journal of Geophysical Research: Solid Earth*, *119*, 8688–8707. <https://doi.org/10.1002/2014JB011526>
- Wu, S. M., Ward, K. M., Farrell, J., Lin, F. C., Karplus, M., & Smith, R. B. (2017). Anatomy of Old Faithful from subsurface seismic imaging of the Yellowstone Upper Geyser Basin. *Geophysical Research Letters*, *44*, 10,240–10,247. <https://doi.org/10.1002/2017GL075255>

References From the Supporting Information

- Crampin, S. (1978). Seismic-wave propagation through a cracked solid: Polarization as a possible dilatancy diagnostic. *Geophysical Journal International*, *53*(3), 467–496. <https://doi.org/10.1111/j.1365-246X.1978.tb03754.x>
- Hu, G., Menke, W., & Powell, C. (1994). Polarization tomography for P wave velocity structure in southern California. *Journal of Geophysical Research*, *99*(B8), 15,245–15,256. <https://doi.org/10.1029/93JB01572>
- Jurkevics, A. (1988). Polarization analysis of three-component array data. *Bulletin of the Seismological Society of America*, *78*(5), 1725–1743.
- Ozacar, A. A., & Zandt, G. (2004). Crustal seismic anisotropy in central Tibet: Implications for deformational style and flow in the crust. *Geophysical Research Letters*, *31*, L23601. <https://doi.org/10.1029/2004GL021096>
- Park, S., & Ishii, M. (2018). Near-surface compressional and shear wave speeds constrained by body-wave polarization analysis. *Geophysical Journal International*, *213*(3), 1559–1571. <https://doi.org/10.1093/gji/ggy072>
- Shapiro, N. M., Campillo, M., Stehly, L., & Ritzwoller, M. H. (2005). High-resolution surface-wave tomography from ambient seismic noise. *Science*, *307*(5715), 1615–1618. <https://doi.org/10.1126/science.1108339>